

Deep Instance Segmentation with High-Resolution Automotive Radar

Jianan Liu^{1*}, Weiyi Xiong^{2*}, Liping Bai², Yuxuan Xia³, Bing Zhu^{2†}

¹Derimis Tech., Gothenburg, Sweden

²Beihang University, Beijing, China

³Chalmers University of Technology, Gothenburg, Sweden

Abstract—Automotive radar has been widely used in the modern advanced driver assistance systems (ADAS) and autonomous driving system as it provides reliable environmental perception in all-weather conditions with affordable cost. However, automotive radar usually only plays as an auxiliary sensor since it hardly supplies semantic and geometry information due to the sparsity of radar detection points. Nonetheless, with the development of high-resolution automotive radar in recent years, more advanced perception functionality like instance segmentation, which has only been well explored using Lidar point clouds, becomes possible by using automotive radar. Its data comes with rich contexts such as Radar Cross Section (RCS) and micro-doppler effects, which may potentially be pertinent, and sometimes can even provide detection when the field of view is completely obscured. Therefore, the effective utilization of radar detection points data is an integral part of automotive perception. The outcome from instance segmentation could be seen as comparable result of clustering, and could be potentially used as the input of tracker for tracking the targets. In this paper, we propose two efficient methods for instance segmentation with radar detection points, one is implemented in an end-to-end deep learning driven fashion using PointNet++ framework, and the other is based on clustering of the radar detection points with semantic information. Both approaches can be further improved by implementing visual multi-layer perceptron (MLP). The effectiveness of the proposed methods is verified using experimental results on the recent RadarScenes dataset.

Index Terms—ADAS, autonomous driving, environmental perception, instance segmentation, semantic segmentation, clustering, classification, automotive radar, deep learning

I. INTRODUCTION

IN the field of autonomous driving, automotive radar plays an important role in environmental perception due to its affordable costs, inherent measuring of object relative speed, and reliability in all-weather conditions, as compared to camera and Lidar. The data representation of an automotive radar is usually a set of detection points (or a point cloud), which are generated by pre-processed raw radar data, typically in the form of a range-Doppler map or a range-azimuth heatmap. Compared to Lidar points, radar points usually provide more information, e.g. velocity (Doppler) and the radar cross section (RCS) values. In addition, radar points are much sparser than Lidar points due to the low resolution of radar, resulting in a lack of semantic and geometric information. Thus, it may not be suitable to directly apply methods developed for Lidar points to radar points.

A common way to process point clouds is to either transform point clouds into 3D grid-like representation called voxel or 2D grid-like representation in the bird eye's view (BEV), or project them into range view[1], and then use CNN to perform classification, detection or segmentation. The main problems of above methods are the high computational and memory cost, and quantization error introduced during the point-to-voxel/pixel transformation. In addition, early stages of CNN has difficulty in capturing the spatial interactions of radar points due to their sparsity, and thus such methods may not be suitable for radar point cloud. Another common way is to use raw points as input, regarding spatial coordinates as part of the features and putting them in the channel dimension [2–5]. This method is more efficient and could overcome the other problems that the former confronted with. Typical examples of the second method include the PointNets [2, 3], and in this work we choose to use PointNet++ [3], as the backbone of our proposed network.

The main contributions are summarized as follows:

- We propose two strategies for automotive radar-based instance segmentation. One is end-to-end instance segmentation with a modified loss function of Similarity Group Proposal Network (SGPN) [4]; the other is semantic segmentation based clustering, and we add a “center shift vectors prediction” branch to the semantic segmentation version of PointNet++ [3] to improve the performance.
- We also design enhanced version of both strategies by incorporating visual Multi-Layer Perceptron (MLP) [6–8], which greatly facilitates the perceptual capability of global information of radar detection points in each frame.
- Experimental results on the recent RadarScenes dataset [9] show that the proposed strategies outperform the baseline (i.e. clustering based classification) by a large margin. Specifically, our selected method attains 88.5% mCov (mean coverage) and 85.2% mAP_{0.5} (mean average precision), which is 9.0% and 9.2% higher than the baseline, respectively.

The rest of this paper is organized as follows. Section II lists related works of different clustering methods, visual MLPs, radar-based perception, as well as neural networks processing point cloud data, such as PointNet, is introduced. Section III describes our two radar-based instance segmentation strategies and their enhancement. Experimental results on

*Both authors contribute equally to the work and are co-first authors.

†Corresponding author.

the RadarScenes dataset are shown and analysed in Section IV. Finally, Section V summarizes the paper and presents promising future work directions.

II. RELATED WORKS

A. DBSCAN and its modification

As mentioned earlier, the generic method of radar-based instance segmentation is clustering based classification. Among different clustering methods, DBSCAN (Density-Based Spatial Clustering of Applications with Noise) [10] algorithm is more suitable for radar detection points. To get better performance, [11] proposed REDBSCAN (Radar Elliptical Density-Based Spatial Clustering of Applications with Noise) by leveraging the radar resolution in clustering. However, this method only use the spatial coordinates. To make fully use of all features of a point, other modified DBSCAN algorithms are proposed. [12] take velocity and the received power into consideration and change the distance metric by using certain footprint. Although not for radar points exclusively, ST-DBSCAN [13] is also devised to process spatial-temporal data, where the time information of points can be seen as a non-spatial feature.

B. Point cloud processing

Point clouds are sporadic and permutation invariant, making effective information extraction challenging. While the image processing techniques, such as 2D convolution, can be extrapolated into the realm of 3D point cloud data processing, the outcomes of such approaches turn out to be ineffective.

PointNet [2] and the subsequent variants [3] are network structures designed specifically for point cloud data, where the input data points are projected into a higher dimension space before going through a permutation invariant function, e.g., a max pooling function, for feature extraction. For classification tasks, the outcome of the max pooling function is utilized for the final prediction, whereas for segmentation tasks, the output of the max pooling function is then combined with other information during the feature propagation layers, and the network also outputs the classification of each data point.

As opposed to taking all the data points as the input of the first layer, as does PointNet, PointNet++ seeks to imitate the convolution layer of 2D images, in an attempt to capture the local context. To achieve this, a Set Abstraction (SA) layer is used to sample, group points and capture local structure. Furthermore, the Feature Propagation (FP) layer is devised to propagate features from sampled points to original points and get point-wise features, for the purpose of segmentation.

PointNet and PointNet++ do not provide the function of direct instance segmentation, but some efforts have been made toward this direction. For instance, SGPN [4] takes PointNets as its backbone and introduce a similarity matrix for instance segmentation. And HAIS [5], a semantic segmentation based clustering method, adopts hierarchical aggregation to progressively generate instance proposals, so as to overcome traditional clustering problems.

C. Visual MLPs

Attention-based transformers [14–16] are popular approaches for computer vision tasks, but some recent works prove that network based on only MLPs achieve comparable performance [8]. MLP-mixer [7] replaces the the multi-head self attention [17] with a linear layer implemented on the spatial dimension. To make the MLP flexibility to receive images of different sizes, cycle-MLP [18] propose a cycle Fully Connected (FC) layer and use it to change the spatial MLP in MLP-mixer. However, as the data structure of images and point clouds are different, such method cannot be applied to our work without voxelizing the point cloud. gMLP [8] discards the multi-head self attention in transformer and add a spatial gating unit to capture spatial interaction. Taking the inspiration from self-attention, external attention [6] uses two linear layers with a double normalization in between, to reduce the computational complexity.

D. Automotive radar-based perception

Automotive radar-based perception, including semantic segmentation, clustering, instance segmentation, object detection and tracking, has played an important role in the modern ADAS and autonomous driving system.

With the availability of large-scale radar datasets [9], deep learning methods have been explored for automotive radar-based perception. For Example, the radar detection points are used as input format to semantic segmentation task [19], together with occupancy grid representation of environments [20, 21]. Such detection points representation of radar data is also employed for object detection and tracking purpose. [22] modifies the PointNets for object detection but only one class (cars) are considered. [23] performs detection and tracking by adopting combinations of networks such as PointNet++, FPN and ResNet.

On the other hand, compared to radar detection points based object detection, better performance can be obtained by leveraging the richer feature information contained in the raw radar data like range-azimuth heatmap, which is demonstrated by [24]. In addition, [25] segments the radar data semantically in multi-view representations of range-Doppler-azimuth 3D cube.

III. PROPOSED METHODS

The most commonly used framework for automotive radar-based perception is to first extract the state information of each object by performing either clustering or instance segmentation on radar detection points, and then employ such state information as input to the tracking filter for refinement of localization information and provision of ID for each object. The performance of the first stage module, i.e., clustering or instance segmentation, becomes the bottleneck of entire perception pipeline since traditional clustering algorithm, e.g., DBSCAN, can only make use of the geometry information, thus leading to poor clustering and subsequent tracking results. Specifically, without carefully hand-crafted hyper-parameters, DBSCAN can easily cluster points belonging to multiple small and closely-spaced targets into one instance, or cluster the

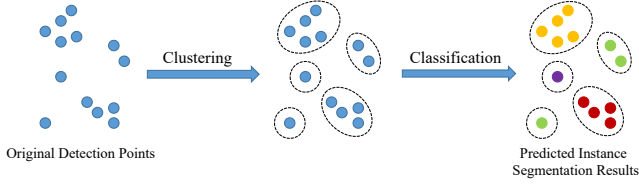


Fig. 1. Illustration for the process of baseline. Different colors denote different classes, where points in the same circle belong to the same instance.

points from a large target into several separate instances. In order to tackle such problem, we propose two deep learning based strategies for automotive radar-based instance segmentation by directly processing the detection points, namely end-to-end instance segmentation and semantic segmentation based clustering. The proposed strategies are based on radar detection points rather than raw level radar data (e.g., the range-Doppler map or range-azimuth heatmap). These strategies could be easily adopted into any automotive radar-based perception pipeline as radar detection points, unlike raw level radar data, can be accessible from any automotive radar product.

In this section, the widely accepted “clustering first classification later” strategy for automotive radar-based instance segmentation, is first introduced as baseline. Then our proposed end-to-end instance segmentation and semantic segmentation based clustering strategies are described. At last, the enhanced versions by incorporating MLPs, which greatly improve the performance of our proposed methods, are analyzed.

A. Clustering based Classification

The common-used method for radar-based instance segmentation is clustering based classification. As illustrated in Fig. 1, the input point cloud is clustered first, and then each cluster is sent into a classifier (e.g. support vector machine or random forest classifier) to get the predicted class of it.

In this work, we choose DBSCAN for clustering and use random forest classifier to predict scores for all classes. The random forest classifier takes hand-crafted features of a cluster that represent the statistics of range, azimuth, Doppler and RCS, such as their mean and standard deviation, etc., are used as input.

B. End-to-End Instance Segmentation

To implement instance segmentation in a deep learning driven fashion, our model is built upon SGPN [4], see Fig. 2 for an illustration. By connecting three heads to PointNet++, such model predicts a similarity matrix S to estimate the how likely any pair of two points belong to the same instance, a similarity confidence map M_{CF} to estimate the uncertainty of similarity results, and a semantic segmentation map M_{SEM} to provide the semantic information estimation of every point.

The loss functions of S and M_{SEM} remain as double hinge loss and cross entropy loss. However, the binary cross entropy loss (BCE), instead of the mean square error (MSE, or l_2),

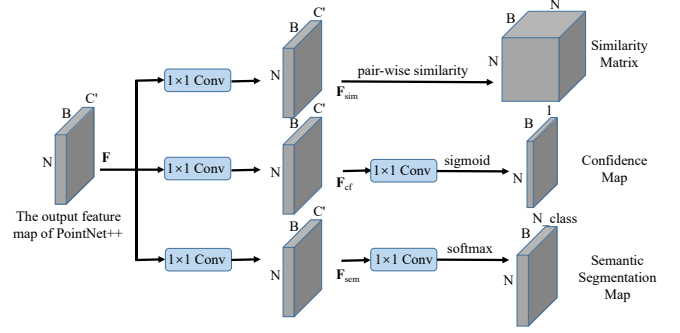


Fig. 2. The heads of our instance segmentation model.

is set as the loss function of M_{CF} to facilitate uncertainty modelling, i.e.,

$$L_{CF} = -\frac{1}{N} \sum_{i=1}^N [iou_i \times \log(M_{CF,i}) + (1 - iou_i) \times \log(1 - M_{CF,i})] \quad (1)$$

where N is the number of predicted group (also the number of points) in a frame, $M_{CF,i}$ is the i -th row of confidence map, and iou_i is the IoU (Intersection over Union) between the ground truth group and the i -th predicted group. Specifically,

$$IoU(g, p) = \frac{|g \cap p|}{|g \cup p|} \quad (2)$$

where g denotes the set of points belonging to a ground truth instance, and p is the set of points in a predicted group.

C. Semantic Segmentation based Clustering

Another way to implement instance segmentation is to reverse the operation order of baseline, i.e., semantic segmentation (point-wise classification) based clustering. It's intuitive that clustering points with semantic information may achieve better performance. For instance, there may be more than 10 detection points from a large vehicle and the distances between these detection points could be larger than those from a two-wheeler, while a pedestrian may only have one detection point. Therefore, it is a good strategy to use different clustering parameter settings for different classes. Specifically, we first let the network model concentrates on semantic segmentation, and then we apply the clustering for each group of detection points with the same semantic information.

As standalone PointNet++ based semantic segmentation hardly provides excellent results for radar detection points [19] due to the sparsity of radar detection points, similar to [5], we add a center shift vectors prediction branch to estimate the offset between every point and the geometric center of corresponding ground-truth instance. In this way, the detection points are assembled by shifting toward the center of the instance they belong to, and thus becoming easier to be clustered. Since the detection points do not carry systematic RCS information like the other two, we carefully tailor the center shift vectors prediction branch such that only coordinate and velocity are used as input to predict the center shift vector for each radar detection point. The architectures of the

prediction heads for our model are just two-layer MLPs, as illustrated in Fig. 3.

The total loss should take into account both the L_{SEM} and L_{SHIFT} . Specifically, L_{SEM} is the cross entropy loss for semantic segmentation head. Instead of using l_2 loss like [5], we define the loss for prediction of center shift vectors, L_{SHIFT} , as the summation of the Cosine Similarity (CS) loss and Normalized Inner Product (NIP) loss, to fully explore the offset shifting generated from feature vectors in the latent space, by leveraging the multi-dimension physical feature information from radar. The exact expressions of L_{CS} and L_{NIP} are

$$L_{CS} = [1 - \text{cosine_similarity}(\Delta x_{pred}, \Delta x_{gt})]$$

$$L_{NIP} = \left| \frac{\text{inner_product}(\Delta x_{pred}, \Delta x_{gt})}{\|\Delta x_{gt}\|^2 + \epsilon} - 1 \right| \quad (3)$$

where ϵ is a small positive number (e.g., $1e-5$) used to prevent zero-division, while Δx_{pred} and Δx_{gt} denote the predicted center shift vector between every detection point and the geometric center of corresponding instance and its ground truth value, respectively. As shown in (3), the CS loss tries to make the included angle approach its ground truth, and the NIP loss is devised for length approximation. Compared to l_2 loss, our loss function for center shift vectors leads to a significant improvement in semantic segmentation of radar detection points, which can be seen in Section IV.

Finally, the total loss is the weighted sum of L_{SEM} and L_{SHIFT} , i.e.,

$$L = L_{SEM} + \alpha L_{SHIFT} \quad (4)$$

$$= L_{SEM} + \alpha (L_{CS} + L_{NIP})$$

where $\alpha > 0$ is a factor that adjusts different losses to the similar order of magnitude, which is beneficial for training multi-task networks.

During inference time, the predicted center shift vectors are used for pushing the detection points towards the center of the instances that they belong to. Since the detection points assigned with different semantic information are scarcely belong to the same instance, we implement several clustering approaches with different parameter settings in parallel to estimate the final instances, one for each semantic group, which gathers all the shifted detection points with the same estimated semantic information. The entire procedure is illustrated in Fig. 4.

D. Enhancement with visual MLPs

Attention-based visual transformers for image processing and perception are extensively studied in recent years, and some of them have been investigated on point cloud datasets. For example, [26] applies 10 different attentions/transformers to point cloud data, making comparisons among them according to their structure and performance. However, as a promising alternative of visual transformers, hardly any of the visual MLPs is used for point cloud data processing. Compared to transformer architectures, the modules in visual MLPs are consistent with the PointNet++ MLP framework, which makes the combination of these two modules easy. In

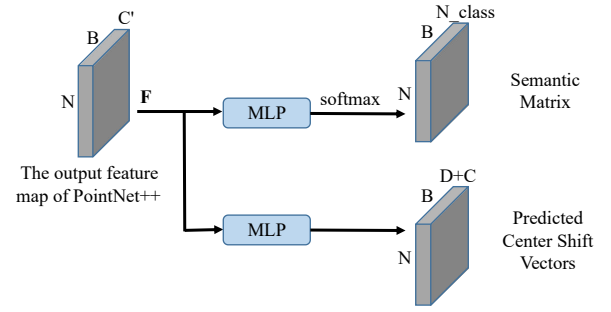


Fig. 3. The heads of our semantic segmentation model. The semantic segmentation branch predicts per-class score for every point, and for center shift vectors branch, the difference between each point and the center of its instance is predicted.

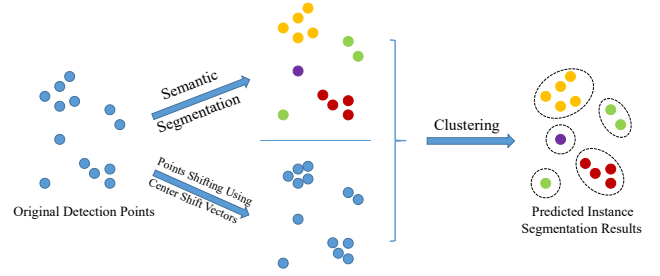


Fig. 4. Illustration for the process of Semantic Segmentation Based Clustering. Different colors denote different classes, where points in the same circle belong to the same instance.

this work, we integrate visual MLPs into our work by adding an MLP block after each SA and FP layer in PointNet++. The extracted feature vectors are fed into an MLP block for down-sized feature refinement and propagated into next layer in the encoder of network. In the decoder, the up-sampled feature vectors are also strengthened by an MLP block to achieve better representations in the latent space. The entire structure of the enhanced network is shown in Fig. 5.

The MLP block in Fig. 5 is used to propagate multiple feature vectors, and it can be any visual MLP, e.g. MLP-Mixer [7], external attention [6], gMLP [8]. In this work, the gMLP (MLP with gating units) is used. Note that in radar detection

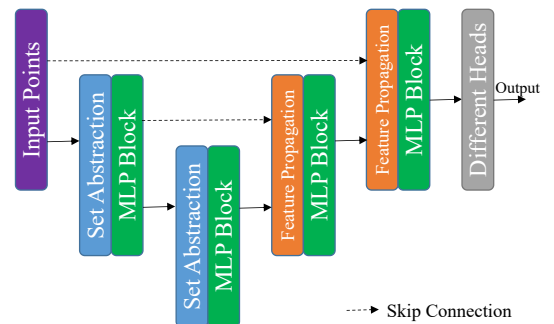


Fig. 5. The structure of the MLP based PointNet++ network. The MLP block can be gMLP, MLP-Mixer, external attention and other MLP blocks that can take in multiple feature vectors.

point representations, instance and semantic information of different objects can potentially be represented by both the number of points from the same instance. For example, the size of instance could be represented by the number of reflected points from the object, and the attributes (channel) information from a group of points, e.g., the points from the same instance are likely to carry similar velocity and RCS. In addition, the position differences between points from the same instance also denote the size of instance and its type. Therefore, the MLP-Mixer module can provide more hidden information by extracting the global features from channel-wise and position-wise combinations separately. Furthermore, as an improved version of MLP-Mixer, gMLP combines the spatial gating mechanism with MLP-Mixer, and through this it may provide more flexibility to tune the feature vectors, and therefore the interaction between number of detection points and features per point could be further improved. The performance of the network with different visual MLPs will be compared and analysed in Section IV.

IV. EXPERIMENTS AND RESULTS

A. Dataset

We choose to validate our idea over the RadarScenes [9] dataset, which contains data from four front-mounted near-range radars, one camera, and one odometer. The four radars are 77 GHz near field automotive radar with a detection range of up to 100 meters. Each radar covers a $\pm 60^\circ$ field of view and radar one to four is mounted at the front end of the vehicle at 85° , 25° , -25° , -85° to the driver, respectively. The data stream is timestamped so that we can use the ego-coordinate of any vehicle as the anchor coordinate system and synchronize information from all four radars into one frame. On average, the frame rate is 17Hz. Each frame contains points ranging from 28 to over 1000 (on average there are 158 points per frame). The illustration of mounting positions of four radars and corresponding field of view (FOV) can be seen in Fig. 6.

The radar data consists of temporal, positional, and id information, in both Cartesian and polar coordinates. Four are germane to our experiment: radar cross-section (*RCS*) in dBsm; *vr_compensated* in m/s, which is the radial velocity for this detection but compensated for the ego-motion; *x_cc* in meters, which is the position of the detection horizontal to the car in the car coordinate system (origin is at the center of the rear-axle); *y_cc* in meters, which is the position of the detection orthogonal to the car in the car coordinate system (origin is at the center of the rear-axle).

In general, RadarScenes contains real-world radar detection point clouds from different driving environments, which are manually annotated with a class, an instance ID and other information. More specifically, there are more than 4 hours' recording in this dataset and it's composed of 158 sequences, but in order to reduce difference among training set, validation set and testing set, we shuffle the frames and split them by the proportion of 8:1:1.

B. Implementing Details

All experiments adopts similar settings: the batch size is 512, the initial learning rate is $1e-3$ and the optimizer is Adam.

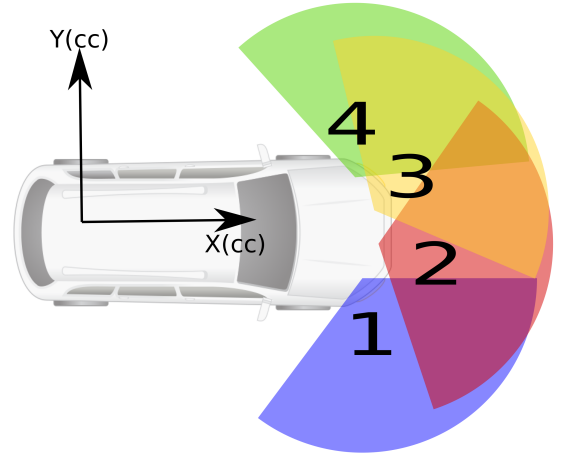


Fig. 6. The illustration of radars in radarscenes dataset.

The learning rate restarts every 20 epochs with the scheduler of Cosine Annealing Warm Restarts.

Although there are 12 classes of objects in RadarScenes, we choose the 5-class setting (i.e. car, pedestrian, group of pedestrians, large vehicles and two wheeler) that merge similar classes into one, for the lack of data in some classes. In addition, we do not use the static points, in consideration that the overwhelming majority of the detection points in the dataset is static, and the accuracy will be high enough if the model learns an all-static prediction.

To solve another problem that every frame has different number of points (for the convenience of expression, we denote the number of points in i -th frame as N_i), points are sampled randomly in a frame. Some statistics are obtained such as $\max(N_i)$ and $\text{mean}(N_i)$, which help determine the sample size. Explicitly, in training, the sample size should be larger than most N_i s because N_i is usually very small, but there is no need to be larger than $\max(N_i)$ as it will improve the computational cost. However, while inferring, the sample size must be larger than $\max(N_i)$, otherwise some of the detection points will be missing. In practice, the number of non-static points in a frame varies from 1 to 173, and less than 0.4% of frames have more than 100 points, so we set the sample size as 100 in training and 200 in testing, except the gMLP based network, whose model parameters contain the sample size so 200 is set in both training and testing.

By sampling (or repeating), there are 100 non-static points in each frame. We approximate the FOV as a $100\text{m} \times 100\text{m}$ field, taking into account the configuration and technical specification of the four near field radars. Based on these numerical structures, we stipulate the PointNet++ segmentation network [3] to have two SA Layers and two corresponding FP Layers. The number of sampled points for the first SA Layer is set to be 64, each with radius 8m. These parameters are designed such that all the sampling cycles would cover the entire FOV

with appropriate overlapping, i.e.

$$n\pi r^2 > S_{FOV}$$

where n is the number of sampled points and r denotes the radius, while S_{FOV} is the area of FOV.

The density of data points at each frame is 200/64, therefore, there are on average 3.1 data points in each sampling cycle. The sampling number is set to be 8 which is larger since the max pooling operation of the PointNet++ network is duplication insensitive and we want to guarantee no under-sampling takes place. This parameter design logic is extended to the second SA Layer, only with the input data to be reduced to 64.

In practice, we use the same network architecture for both instance segmentation and semantic segmentation:

$$\begin{aligned} SA(64, 8, [8, 32, 64]) \\ SA(16, 16, [64, 128, 256]) \\ FP(64, 32) \\ FP(32, 32, 16) \end{aligned}$$

where the notations are the same as those in PointNet++ [3]. Specifically, $SA(K, r, [l_1, \dots, l_d])$ means a set abstraction level sampling K points, and the searching radius for each sampled point is r , which is followed by a PointNet of d 1×1 convolution layers whose output channels are l_1, \dots, l_d , respectively; $FP(l_1, \dots, l_d)$ is a feature propagation level with d 1×1 convolution layers. The final output of PointNet++ backbone is denoted as \mathbf{F} . Beware for the enhanced models, the visual MLP block does not change the dimension of output feature vectors thus it could be appended in following of each SA or FP directly.

The structure of heads for instance segmentation are shown below:

$$\begin{aligned} \mathbf{F}_{SIM} &= conv(\mathbf{F}, 16), \mathbf{S}_{ij} = \|\mathbf{F}_i - \mathbf{F}_j\|_2 \\ \mathbf{F}_{CF} &= conv(\mathbf{F}, 16), \mathbf{M}_{CF} = conv(\mathbf{F}_{CF}, 1) \\ \mathbf{F}_{SEM} &= conv(\mathbf{F}, 16), \mathbf{M}_{SEM} = conv(\mathbf{F}_{SEM}, n_{class}) \end{aligned}$$

where $conv(\mathbf{X}, l)$ denotes a 1×1 convolution layer whose input is \mathbf{X} and output channel l , \mathbf{F}_k is the feature vector of the k -th point, \mathbf{S}_{ij} is the similarity value in position (i, j) of \mathbf{S} , and n_{class} is the number of classes, which is 5 in our experiment. BatchNorm, ReLU and Dropout are used between two consecutive convolution layers.

The structure of heads for semantic segmentation are as follows:

$$\begin{aligned} \mathbf{F}_{SEM} &= conv(\mathbf{F}, 16), \mathbf{M}_{SEM} = conv(\mathbf{F}_{SEM}, n_{class}) \\ \mathbf{F}_{SHIFT} &= conv(\mathbf{F}, 16), \mathbf{M}_{SHIFT} = conv(\mathbf{F}_{SHIFT}, n_{dim}) \end{aligned}$$

where \mathbf{M}_{SHIFT} is the predicted center shift vectors and n_{dim} denotes the dimension of raw radar detection points.

C. Evaluating Metrics

We perform experiments on RadarScenes to evaluate the effectiveness of our strategies. The spatial coordinates, velocities (compensated) and RCS values are used as input, while mean coverage (mCov) and mean average precision with the

TABLE I
THE FOUR RELATIONSHIPS BETWEEN THE PREDICTION AND GROUND TRUTH IN CLASSIFICATION TASKS

Relationships	Predicted Class = Actual Class ?	
	True	False
Actual Class	True Positive (TP)	False Negative (FN)
Other Classes	False Positive (FP)	True Negative (TN)

TABLE II
THE PRECISION AND RECALL OF ALL PREDICTIONS

Orders	1	2	3	4	5	6
Predictions	TP	TP	FP	TP	FP	TP
Precision	1/1	2/2	2/3	3/4	3/5	4/6
Recall	1/5	2/5	2/5	3/5	3/5	4/5

IoU threshold of 0.5 ($mAP_{0.5}$) on original detection points are reported for final instance prediction.

The mCov can be calculated as follows:

$$mCov(G, P) = \frac{1}{|G|} \sum_{g \in G} \max_{p \in P} IoU(g, p) \quad (5)$$

where G is the set of ground truth instances and P is the set of predicted instances, while g and p denotes the element (a set of points belonging to an instance) of sets G and P , respectively. $IoU(g, p)$ is defined in (2).

In other word, IoU reflects the accuracy for a certain instance and its prediction, and mCov is the average accuracy for all instances. The closer mCov is to 1, the performance of the model is better.

Before explaining mAP, some terms need to be introduced. For classification tasks, there are four relationships between the predicted class and the ground truth, and we can summarize them into Table I.

The precision and recall are defined as (6).

$$precision = \frac{TP}{TP + FP} \quad recall = \frac{TP}{TP + FN} \quad (6)$$

Notably, precision and recall is defined on a certain class.

AP is a metric for segmentation or detection that takes both precision and recall into consideration. It first sorts the predictions by their confidence scores (usually the predicted probability of this class) from large to small, then calculate the IoU between each prediction and all ground truths. If an IoU between a prediction and a ground truth is larger than a certain threshold, we mark the prediction as TP. Then we traverse each prediction in order, and a precision-recall curve is drawn. For example, a sorted and marked list of predictions for an instance segmentation task is $[TP, TP, FP, TP, FP, TP]$, and there are 5 objects belonging to this class in ground truth. If we look at the 3rd prediction, the precision can be calculated as 2/3 because there are 2 TPs in the first 3 predictions; the recall can be calculated as 2/5 because there are 2 TPs while 5 instances exist. The precision and recall of each prediction is listed in Table II.

After getting the precisions and recalls, we establish a precision-recall coordinate system whose horizontal axis is recall and vertical axis is precision. Then a broken line called PR curve to connect all points in order is drawn, and the area of the figure enclosed by the precision-recall curve and the

TABLE III
RESULTS OF DIFFERENT STRATEGIES FOR INSTANCE SEGMENTATION ON TEST DATA

	Methods	mCov(%)	mAP _{0.5} (%)	#Params	Inference Time
Baseline: Clustering & Classification	DBSCAN + Random Forest Classifier	79.54	76.09	-	17.1ms
End-to-End Instance Segmentation	SGPN (l_2 loss for \mathbf{CF})	77.32	73.21	9.541M	63.8ms
	SGPN (our BCE loss for \mathbf{CF})	79.91	76.15		
Semantic Segmentation & Clustering	PointNet++ + DBSCAN	82.21	77.96	9.422M	27.4ms
	PointNet++ (with csv head, l_2 loss) + DBSCAN	82.38	78.17	9.493M	28.7ms
	PointNet++ (with csv head, CS&NIP loss) + DBSCAN	82.78	79.38		

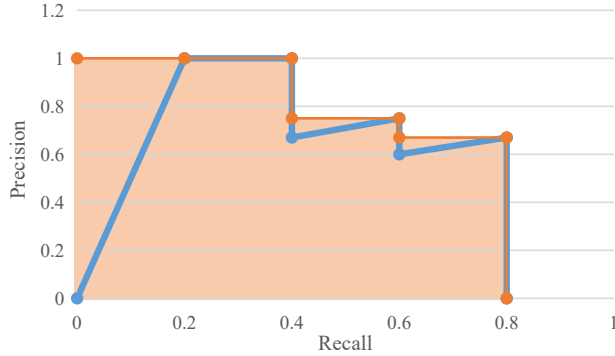


Fig. 7. The PR curve of the example. The blue line is the original PR curve and the orange line is the adjusted PR curve. The area of the shaded part is AP.

axes is calculated. The result is AP, but in practice, people usually adjust the longitudinal coordinate of a point as the maximum value of that of points on its right. Fig. 7 illustrates the original and the adjusted PR curve of the previous example.

Finally, we calculate the average of APs for all classes and get the mAP for the task. The larger mAP is, the better the performance is.

D. Experimental Results and Analysis

Table III presents the result of baseline and our two strategies without any visual MLP enhancement. The performance of the SGPN based end to end instance segmentation improves about 3% by simply modifying its loss function from l_2 loss to BCE loss. However, such deep learning based end to end instance segmentation strategy only outperforms the baseline a little, but trebles the inference time. In contrast, the semantic segmentation based clustering strategy reaches the mCov at 82.21% and mAP at 77.96% without increasing too much inference time, while further improvement can be made by adding a center shift vectors prediction branch to PointNet++ using CS and NIP loss to achieve 82.78% for mCov and 79.38% for mAP. Note both number of parameters and inference times for all the models are also given, and the inference time is defined as the average time cost when performing instance segmentation on test dataset using CPU.

The experimental results of the enhanced models are summarized in Table IV. To show the effectiveness of our proposed semantic segmentation based clustering with gMLP enhancement strategy, we also use external attention and self attention for semantic segmentation network for comparison.

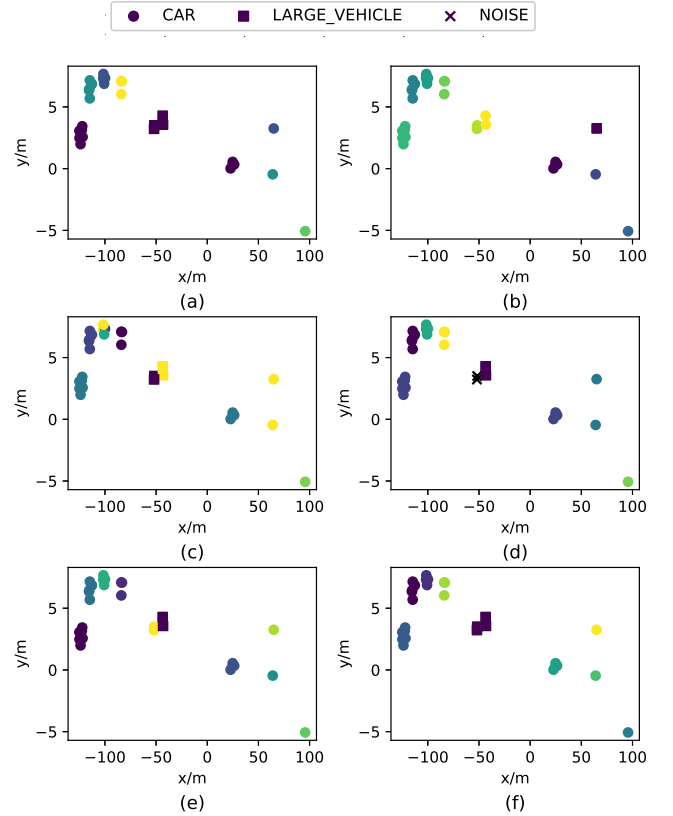


Fig. 8. Visualization of typical instance segmentation results by using different strategies. Different shapes represent different semantics, and different colors in the same class (same shape) denotes different instances. (a) Ground Truth for instance segmentation. (b) Instance segmentation results using the strategy of clustering based classification. (c) Instance segmentation results using the strategy of end-to-end instance segmentation. (d) Instance segmentation results using the strategy of end-to-end instance segmentation with gMLP. (e) Instance segmentation results using the strategy of semantic segmentation based clustering. (f) Instance segmentation results using the strategy of gMLP enhanced semantic segmentation based clustering.

Compared with the original version, the gMLP based model performs better by nearly 6%, while the self attention and external attention based model only gets an improvement of about 3% and 2%, respectively, with similar inference time and number of parameters. Notably, by attaching a tiny attention module to the spatial gating unit, the aMLP based model makes further improvement while slight increasing the inference time and number of parameters used. For SGPN based end to end instance segmentation, gMLP also makes it outperforms the baseline by around 5%, but the inference time increases dramatically thus makes the gMLP enhancement of

TABLE IV
RESULTS OF DIFFERENT ENHANCED MODELS ON TEST DATA

	Methods	mCov(%)	mAP _{0.5} (%)	#Params	Inference Time
End-to-End Instance Segmentation	SGPN	79.91	76.15	9.541M	63.8ms
	gMLP based SGPN	84.11	81.09	15.075M	336.3ms
Semantic Segmentation based Clustering	PointNet++ with csv head + DBSCAN	82.78	79.38	9.493M	28.7ms
	gMLP based PointNet++ with csv head + DBSCAN	88.54	85.24	14.928M	32.5ms
	aMLP based PointNet++ with csv head + DBSCAN	89.53	86.97	18.448M	35.4ms
	External Attention based PointNet++ with csv head + DBSCAN	85.23	81.41	11.214M	31.2ms
	Self Attention based PointNet++ with csv head + DBSCAN	85.85	82.32	12.375M	32.0ms

such strategy infeasible in practice. All the models in Table III and Table IV occupy from less than 1MB to 5MB of the storage space, thus making such strategies feasible to be deployed into embedded radar based perception systems. However, only semantic segmentation based clustering with gMLP enhancement strategy improves the performance in mAP and mCov greatly while still maintains the inference time fairly low thus it can be executed in real-time.

Typical examples of instance segmentation results by using different strategies is visualized in Fig. 8. It is obvious the baseline strategy clustering based classification can easily obtain the incorrect instance and semantic estimation, the deep learning based end to end instance segmentation strategy and its gMLP enhanced version could correct estimation partly but generate other improper predictions, yet the semantic segmentation based clustering provide clearly better estimation and the one with gMLP enhancement achieves 100% correct prediction for this particular case. Another illustration of results of consecutive frames by using our proposed semantic segmentation based clustering with gMLP enhancement strategy could be seen in Fig. 9, it evidences most of the instances could be segmented perfectly even some of them are spatially very close with each other. However, we can also observe two instances of car are grouped together on the 2nd frame, one car instance is divided into two instances and another car instance is recognized as large vehicle on 3rd frames. Such issues could be potentially solved by incorporating the consistent information from consecutive frames for further study. For example, a car identified at previous frame should not be possible to be recognized as a pedestrian in the current frame.

V. CONCLUSION AND FURTHER WORK

In this paper, we propose two strategies for radar point cloud instance segmentation. One is end-to-end instance segmentation using SGPN, and the other is semantic segmentation based clustering by PointNet++ and DBSCAN. The latter strategy does not only provide better performance in mCov and mAP than the former one, but also much faster while inferring. The inference time of the latter method does not increase much compared to the baseline clustering + classification strategy, whereas the performance shows significantly better.

After we carefully decide the model parameters and compare the effect of different loss functions, an enhancement with gMLP is introduced. The gMLP enhanced semantic segmentation based clustering can provide great improvement in mCov and mAP, but the inference time only increases slightly

compared to the one without gMLP and the requirement of storage space for the corresponding model is less than 5MB, thus makes our proposed gMLP enhanced semantic segmentation based clustering strategy feasible for the real-time embedded radar-based ADAS/AD product.

However, we only consider using detection points within single frame for training the model and predicting the instance information in this study, even if the dataset provides sequences of radar point clouds, i.e. point cloud videos. Taking point clouds of several consecutive frames into account at the same time might enable the model to extract features with consistent information and facilitate learning, which is worth studying in the future.

ACKNOWLEDGMENT

The authors would like to thank...

REFERENCES

- [1] S. Chen, B. Liu, C. Feng, C. Vallespi-Gonzalez, and C. K. Wellington, "3d point cloud processing and learning for autonomous driving," *ArXiv*, vol. abs/2003.00601, 2020.
- [2] C. Qi, H. Su, K. Mo, and L. Guibas, "Pointnet: Deep learning on point sets for 3d classification and segmentation," *2017 IEEE Conference on Computer Vision and Pattern Recognition (CVPR)*, pp. 77–85, 2017.
- [3] C. Qi, L. Yi, H. Su, and L. Guibas, "Pointnet++: Deep hierarchical feature learning on point sets in a metric space," in *NIPS*, 2017.
- [4] W. Wang, R. Yu, Q. Huang, and U. Neumann, "Sgpn: Similarity group proposal network for 3d point cloud instance segmentation," *2018 IEEE/CVF Conference on Computer Vision and Pattern Recognition*, pp. 2569–2578, 2018.
- [5] S. Chen, J. Fang, Q. Zhang, W. Liu, and X. Wang, "Hierarchical aggregation for 3d instance segmentation," *ArXiv*, vol. abs/2108.02350, 2021.
- [6] M.-H. Guo, Z.-N. Liu, T.-J. Mu, and S. Hu, "Beyond self-attention: External attention using two linear layers for visual tasks," *ArXiv*, vol. abs/2105.02358, 2021.
- [7] I. Tolstikhin, N. Houlsby, A. Kolesnikov, L. Beyer, X. Zhai, T. Unterthiner, J. Yung, D. Keysers, J. Uszkoreit, M. Lucic, and A. Dosovitskiy, "Mlp-mixer: An all-mlp architecture for vision," *ArXiv*, vol. abs/2105.01601, 2021.
- [8] H. Liu, Z. Dai, D. R. So, and Q. V. Le, "Pay attention to mlps," *ArXiv*, vol. abs/2105.08050, 2021.

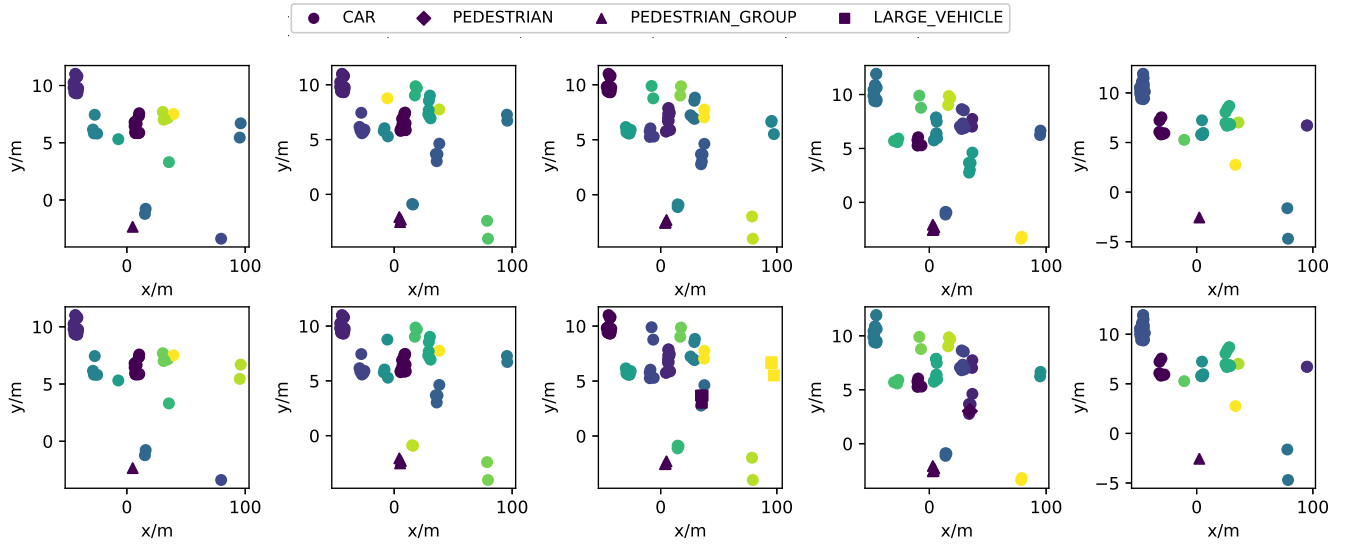


Fig. 9. Visualization of typical instance segmentation results in several consecutive frames. Strategy of gMLP enhanced semantic segmentation based clustering is used to generate these figures. The first row is the ground truth for instance segmentation, and the second row is the predicted instance segmentation results.

- [9] O. Schumann, M. Hahn, N. Scheiner, F. Weishaupt, J. F. Tilly, J. Dickmann, and C. Wöhler, “Radarscenes: A real-world radar point cloud data set for automotive applications,” *ArXiv*, vol. abs/2104.02493, 2021.
- [10] M. Ester, H.-P. Kriegel, J. Sander, and X. Xu, “A density-based algorithm for discovering clusters in large spatial databases with noise,” in *KDD*, 1996.
- [11] R. Zhang and S. Cao, “Robust and adaptive radar elliptical density-based spatial clustering and labeling for mmwave radar point cloud data,” *2019 53rd Asilomar Conference on Signals, Systems, and Computers*, pp. 919–924, 2019.
- [12] T. Wagner, R. Feger, and A. Stelzer, “Modification of db-scan and application to range/doppler/doa measurements for pedestrian recognition with an automotive radar system,” *2015 European Radar Conference (EuRAD)*, pp. 269–272, 2015.
- [13] D. Birant and A. Kut, “St-dbscan: An algorithm for clustering spatial-temporal data,” *Data Knowl. Eng.*, vol. 60, pp. 208–221, 2007.
- [14] A. Dosovitskiy, L. Beyer, A. Kolesnikov, D. Weissenborn, X. Zhai, T. Unterthiner, M. Dehghani, M. Minderer, G. Heigold, S. Gelly, J. Uszkoreit, and N. Houlsby, “An image is worth 16x16 words: Transformers for image recognition at scale,” *ArXiv*, vol. abs/2010.11929, 2021.
- [15] X. Dong, J. Bao, D. Chen, W. Zhang, N. Yu, L. Yuan, D. Chen, and B. Guo, “Cswin transformer: A general vision transformer backbone with cross-shaped windows,” *ArXiv*, vol. abs/2107.00652, 2021.
- [16] Z. Liu, Y. Lin, Y. Cao, H. Hu, Y. Wei, Z. Zhang, S. C.-F. Lin, and B. Guo, “Swin transformer: Hierarchical vision transformer using shifted windows,” *ArXiv*, vol. abs/2103.14030, 2021.
- [17] A. Vaswani, N. M. Shazeer, N. Parmar, J. Uszkoreit, L. Jones, A. N. Gomez, L. Kaiser, and I. Polosukhin, “Attention is all you need,” *ArXiv*, vol. abs/1706.03762, 2017.
- [18] S. Chen, E. Xie, C. Ge, D. Liang, and P. Luo, “Cyclemlp: A mlp-like architecture for dense prediction,” *ArXiv*, vol. abs/2107.10224, 2021.
- [19] O. Schumann, M. Hahn, J. Dickmann, and C. Wöhler, “Semantic segmentation on radar point clouds,” *2018 21st International Conference on Information Fusion (FUSION)*, pp. 2179–2186, 2018.
- [20] R. Prophet, A. Deligiannis, J.-C. Fuentes-Michel, I. Weber, and M. Vossiek, “Semantic segmentation on 3d occupancy grids for automotive radar,” *IEEE Access*, vol. 8, pp. 197 917–197 930, 2020.
- [21] R. Prophet, G. Li, C. Sturm, and M. Vossiek, “Semantic segmentation on automotive radar maps,” *2019 IEEE Intelligent Vehicles Symposium (IV)*, pp. 756–763, 2019.
- [22] A. Danzer, T. Griebel, M. Bach, and K. Dietmayer, “2d car detection in radar data with pointnets,” *2019 IEEE Intelligent Transportation Systems Conference (ITSC)*, pp. 61–66, 2019.
- [23] J. F. Tilly, S. Haag, O. Schumann, F. Weishaupt, B. Duraisamy, J. Dickmann, and M. Fritzsche, “Detection and tracking on automotive radar data with deep learning,” *2020 IEEE 23rd International Conference on Information Fusion (FUSION)*, pp. 1–7, 2020.
- [24] W. Kim, H. Cho, J. Kim, B. Kim, and S. Lee, “Yolo-based simultaneous target detection and classification in automotive fmcw radar systems,” *Sensors (Basel, Switzerland)*, vol. 20, 2020.
- [25] A. Ouaknine, A. Newson, P. P’erez, F. Tupin, and J. Rebut, “Multi-view radar semantic segmentation,” *ArXiv*, vol. abs/2103.16214, 2021.
- [26] S. Qiu, Y. Wu, S. Anwar, and C. Li, “Investigating attention mechanism in 3d point cloud object detection,” *ArXiv*, vol. abs/2108.00620, 2021.